Available online at www.sciencedirect.com
SCIENCE DIRECT®
Polyhedron 22 (2003) 3413–3422
POLYHEDRON
www.elsevier.com/locate/poly

Benzylidyne-capped group 9 trinuclear clusters: synthesis, structure and properties of trirhodium and cobalt–rhodium mixed-metal clusters $[Co_{3-n}Rh_nCp_3(\mu_3\text{-}CPh)_2]$ ($n = 1, 2, 3$)

Masahiro Ebihara [a], Masami Iiba [a], Satohisa Higashi [a], Naoki Tsuzuki [a], Takashi Kawamura [a,*], Tsunenori Morioka [b], Shinji Ozawa [b], Tokio Yamabe [b], Hideki Masuda [c]

[a] *Department of Chemistry, Faculty of Engineering, Gifu University, Yanagido, Gifu 501-1193, Japan*
[b] *Division of Molecular Engineering, Faculty of Engineering, Kyoto University, Kyoto 606-8501, Japan*
[c] *Department of Applied Chemistry, Nagoya Institute of Technology, Showa-ku, Nagoya 466-8555, Japan*

Received 25 July 2003; accepted 1 September 2003

Abstract

The benzylidyne-capped trirhodium and cobalt–rhodium mixed-metal clusters $[M_3Cp_3(\mu_3\text{-}CPh)_2]$ (M_3: Rh_3, **1**; $CoRh_2$, **2**; Co_2Rh, **3**) were synthesized. Complex **1** was prepared from $[CpRh(CO)_2]$ and diphenylacetylene. Complexes **2** and **3** were synthesized by using a mixture of $[CpRh(CO)_2]$ and $[CpCo(CO)_2]$ and separated with silica-gel column chromatography. The molecular structures of **1**, **2** and **3** were determined. The average Rh—Rh distance (2.617(8) Å) in **2** is nearly equal to that in **1** (2.620(13) Å), and the average Co—Rh distance (2.503(16) Å) in **2** is similar to the average of the average Co—Co (2.382(8) Å) length in $[Co_3Cp_3(\mu_3\text{-}CPh)_2]$ (**4**) and the average Rh—Rh distance in **1**. Clusters **2**, **3** and **4** showed a chemically reversible one-electron oxidation and a chemically reversible one-electron reduction response in MeCN. For **1**, a chemically reversible one-electron reduction and irreversible oxidation waves were observed in MeCN, whereas in CH_2Cl_2, two chemically reversible oxidation waves were observed. The oxidation and the reduction potentials shifted to more positive and more negative potential, respectively, with an increase of the number of rhodium atoms. The anionic radical of **3** was generated by the reaction with potassium metal in 2-methyltetrahydrofuran and was examined with ESR. The isotropic hyperfine coupling constant of the ^{59}Co nuclei of $\mathbf{3}^{-\cdot}$ was slightly smaller than that of $\mathbf{4}^{-\cdot}$. Geometry optimization of model complexes $[M_3Cp_3(\mu_3\text{-}CH)_2]$ (M_3: Rh_3, **1′**; $CoRh_2$, **2′**; Co_2Rh, **3′**) was carried out by a density functional theory (DFT) calculation. Assignments of low-energy UV–Vis absorption bands for **1** and **4** are proposed based on transitions of **1′** and $[Co_3Cp_3(\mu_3\text{-}CH)_2]$ (**4′**) calculated by time-dependent DFT.

Keywords: Rhodium complexes; Cobalt complexes; Metal–metal bonds; X-ray structure analyses; Electronic structures; Cyclic voltammetry

1. Introduction

A trinuclear triangle metal unit is a common building framework for transition metal cluster complexes with high nuclearity. Cluster complexes of group 9 metals with cyclopentadienyl groups ($C_5H_{5-x}Me_x$) have been a major field in triangle metal cluster chemistry [1]. Many tricobalt clusters with various capping ligands $[Co_3(C_5H_{5-x}Me_x)_3(\mu_3\text{-}X)(\mu_3\text{-}Y)]^n$ (X, Y = CO, NR, NO, S, etc.; $x = 0, 1, 5$; $n = -1$ to $+2$) have been synthesized. They have 46–51 cluster core valence electrons, the electron count of 48 being in accordance with the noble gas rule. Dahl and co-workers [2–11] have studied the electronic structure of trinuclear clusters. Molecular structures of the 48-electron cluster $[Co_3Cp'_3(\mu_3\text{-}S)_2]^{2+}$ (Cp′ = methylcyclopentadienyl) have been reported to have pseudo-D_{3h} geometries [6]. The 49-electron complex of $[Co_3Cp'_3(\mu_3\text{-}S)_2]^{+}$ has one long and two short Co—Co bonds, whereas two long and one short Co—Co bonds

* Corresponding author. Tel.: +81-58-293-2567; fax: +81-58-230-1893.
E-mail address: kawamura@apchem.gifu-u.ac.jp (T. Kawamura).

0277-5387/$ - see front matter © 2003 Elsevier Ltd. All rights reserved.
doi:10.1016/j.poly.2003.09.001

have been observed in the cyclopentadienyl analog, $[Co_3Cp_3(\mu_3\text{-}S)_2]^+$ [6]. The core structures of the corresponding 50-electron complexes, $[Co_3Cp_3(\mu_3\text{-}S)_2]$ and $[Co_3Cp'_3(\mu_3\text{-}S)_2]$, have been reported to have different types of core structures. Two independent X-ray structure analyses of $[Co_3Cp_3(\mu_3\text{-}S)_2]$ at room temperature have been reported [3,12]. Both of them have D_{3h} core symmetry of which Co—Co distances were 2.687(3) Å [3] and 2.691(4) Å [12], respectively. The structure at 130 K had two short (2.63(1) Å) and one long Co—Co (2.76(1) Å) bonds [12]. On the other hand, in the structure of $[Co_3Cp'_3(\mu_3\text{-}S)_2]$ there were two short Co—Co bonds (average 2.48(1) Å) and one quite long Co—Co distance (average 3.19(1) Å) even at room temperature [6]. Solid-state magnetic susceptibility data showed that $[Co_3Cp'_3(\mu_3\text{-}S)_2]$ is diamagnetic from 6 to 280 K and $[Co_3Cp_3(\mu_3\text{-}S)_2]$ is paramagnetic. However, the investigation of the temperature dependence of the ^{1}H NMR signal in the solution for both of the complexes has indicated the existence of a singlet–triplet spin equilibrium. Based on these results, Dahl and co-workers have concluded that the HOMOs are degenerate for this class of complexes with the 49 and 50 cluster core valence electrons and the substituent on the cyclopentadienyl ligand induced geometrical and electronic structural change of the trinuclear clusters, which may be caused by Jahn–Teller distortion.

The alkylidyne bicapped clusters, $[Co_3(C_5H_{5-x}Me_x)_3(\mu_3\text{-}CR)(\mu_3\text{-}CR')]$, are 48 core valence electron ones. Since the first alkylidyne-bicapped tricobalt cluster $[Co_3Cp_3(\mu_3\text{-}CSiMe_3)(\mu_3\text{-}CCCSiMe_3)]$ was reported by Vollhardt and co-workers [13], X-ray structure analyses, properties and reactivity of the compounds with a variety of alkylidyne ligands have been reported [14–22]. We have discussed the electronic structure of $[Co_3Cp_3(\mu_3\text{-}CPh)_2]$ based on ESR spectra of its anionic and cationic radicals [21]. The substitution of cobalt atoms by rhodium atoms should affect the electronic structure of the trinuclear cluster. Compared with the tricobalt clusters, only a few trirhodium clusters have been synthesized. To our best knowledge, the molecular structure of alkylidyne-capped trirhodium complexes has been reported only for $[Rh_3Cp^*_3(\mu_3\text{-}CH)_2]$ [23]. In this type of trinuclear clusters, metal-atom dependence has not been studied in detail. To examine the metal-atom dependence of the electronic structure of these alkylidyne-capped clusters, we synthesized a series of the trirhodium and cobalt–rhodium mixed-metal clusters, **1**, **2** and **3**, characterized them with X-ray crystallography, and examined their properties. To explore the electronic structures of these complexes, DFT calculations for model complexes **1′**, **2′** and **3′** were carried out. Assignments of UV–Vis absorption bands in low-energy region for homometal clusters, **1** and **4**, are also proposed based on transitions of **1′** and **4′** calculated by TDDFT.

2. Experimental

2.1. Synthesis

2.1.1. General methods

The starting materials, $[CpCo(CO)_2]$ [24] and $[CpRh(CO)_2]$ [25], were prepared by literature methods. Diphenylacetylene and decalin were used as received. Dichloromethane, *n*-hexane and acetonitrile were distilled from CaH_2 before use. Complex **4** was synthesized by following the method of Vollhardt and Fritch [18], purified by silica-gel chromatography and recrystallized from *n*-hexane. Preparation of trinuclear cluster complexes was carried out under an Ar atmosphere and chromatographic separation and purification were made in the air.

2.1.2. $Rh_3Cp_3(\mu_3\text{-}CPh)_2]$ (**1**)

Diphenylacetylene (3.33 g, 18.7 mmol) and $[CpRh(CO)_2]$ (2.52 g, 11.2 mmol) were dissolved in decalin (50 mL). The solution was added intermittently to refluxing decalin (150 mL) over a period of 12 h. Then another decalin solution (100 mL) of diphenylacetylene (6.65 mg, 37.3 mmol) was also added dropwise to the refluxing solution over a period of 3 h. Further 12 h reflux made the solution color black. Decalin was removed by distillation and the residue was extracted by 200 mL of CH_2Cl_2 and then by 250 mL of *n*-hexane. The extracted component was concentrated and loaded onto a silica-gel middle-pressure column (30 mm ϕ, 380 mm length; Merck Si60). The third component (orange) eluted by CH_2Cl_2/*n*-hexane (1/9 v/v) was collected and evaporated to dryness. The complex was then recrystallized from *n*-hexane. Yield 154 mg (6.0%). *Anal.* Calc. for $C_{29}H_{25}Rh_3$; C, 51.06; H, 3.69. Found: C, 51.06; H, 3.56%. ^{1}H NMR ($CDCl_3$, δ in ppm): 5.06 (s, Cp), 7.16 (t, *p*-Ph), 7.22 (t, *m*-Ph), 7.71 (d, *o*-Ph). ^{13}C NMR ($CDCl_3$, δ in ppm): 86.9 (Cp), 125.8, 126.9, 127.7, 162.8 (Ph). IR (KBr disc, in cm^{-1}): 1343 m, 1262 s, 1105 m, 1028 w, 1011 w, 831 s, 791 vs, 729 s, 693 vs, 669 w, 662 m, 634 m.

2.1.3. $CoRh_2Cp_3(\mu_3\text{-}CPh)_2]$ (**2**) and $[Co_2RhCp_3(\mu_3\text{-}CPh)_2]$ (**3**)

A decalin solution (70 mL) containing diphenylacetylene (6.41 g, 36.0 mmol), $[CpRh(CO)_2]$ (2.40 g, 10.7 mmol) and $[CpCo(CO)_2]$ (4.56 g, 25.3 mmol) was added intermittently to 300 mL of refluxing decalin over a period of 12 h. Then another decalin solution (100 mL) of diphenylacetylene (11.9 g, 66.8 mmol) was added to the refluxing solution over a period of 4 h, followed by further 28 h reflux. Decalin was removed by distillation and the residue was extracted by 200 mL of CH_2Cl_2 and then by 250 mL of *n*-hexane. The extracted component was concentrated and loaded on a silica-gel middle-pressure column (30 mm ϕ, 2 × 380 mm length; Merck Si60). Complex **4** (340 mg) was eluted by CH_2Cl_2/*n*-

hexane (1/19 v/v) as the third component (purple). The fourth (reddish purple) and the fifth (brown) bands eluted by CH_2Cl_2/*n*-hexane (1/9 v/v) were **3** and a mixture of **2** and hexaphenylbenzene, respectively. The sixth (orange) band was **1** (25 mg). Each component was collected and evaporated to dryness. Complex **2** was separated from the contaminating hexaphenylbenzene by using a JAI HPLC LC-908 recycling preparative HPLC with a JAIGEL-1H gel-filtration column with a 1,2-dichloroethane eluent. The complexes were recrystallized from *n*-hexane. **2**: Yield 150 mg (4.4%). *Anal.* Calc. for $C_{29}H_{25}CoRh_2$; C, 54.57; H, 3.95. Found: C, 54.32; H, 3.77%. ^{1}H NMR ($CDCl_3$, δ in ppm): 4.28 (s, Co-*Cp*), 5.15 (s, Rh-*Cp*), 7.25 (t, *p*-Ph), 7.34 (t, *m*-Ph), 7.87 (d, *o*-Ph). ^{13}C NMR ($CDCl_3$, δ in ppm): 84.9 (Co-*Cp*), 87.1 (Rh-*Cp*), 125.7, 127.2, 127.5, 164.1 (Ph). IR (KBr disc, in cm^{-1}): 1343 m, 1264 w, 1219 w, 1069 m, 1010 m, 1000 m, 831 s, 790 vs, 729 s, 694 vs, 670 m, 662 m, 635 m. **3**: Yield 540 mg (8.5%). *Anal.* Calc. for $C_{29}H_{25}Co_2Rh$; C, 58.61; H, 4.24. Found: C, 58.91; H, 4.17%. ^{1}H NMR ($CDCl_3$, δ in ppm): 4.39 (s, Co-*Cp*); 5.16 (s, Rh-*Cp*); 7.33 (t, *p*-Ph); 7.43 (t, *m*-Ph); 8.06 (d, *o*-Ph). ^{13}C NMR ($CDCl_3$, δ in ppm): 84.9 (Co-*Cp*); 87.4 (Rh-*Cp*); 125.6, 127.2, 127.3, 165.4 (Ph). IR (KBr disc, in cm^{-1}): 1342 w, 1264 w, 1112 w, 1069 w, 1028 w, 1009 s, 831 m, 803 s, 790 s, 723 s, 695 vs, 670 s, 637 m.

2.2. Measurements

Spectra of ^{1}H and ^{13}C NMR were measured on a JEOL α-400 spectrometer. Electronic absorption spectra were recorded on a Hitachi U-3500 spectrophotometer. IR spectra were measured on a Perkin–Elmer 1600 series FT-IR spectrophotometer. Cyclic voltammograms were measured on a HOKUTO HA-151 potentiostat/galvanostat and a HOKUTO HB-111 function generator with a BAS glassy carbon working electrode, platinum wire counter electrode and an Ag^+/Ag (0.01 mol dm^{-3} $AgNO_3$ in CH_3CN) reference electrode at the potential scan rate of 100 mV s^{-1}. To correct the liquid junction potential, the oxidation potential of ferrocene (Fc) was measured in the same electrolytic solution after each CV measurement and the electrode potentials were converted into those relative to Fc^+/Fc. ESR was measured on a JEOL PE-2X spectrometer. MTHF was dried on an NaK alloy and transferred to a sample tube under a vacuum. Anionic radicals were generated in contact of an MTHF solution of a complex with potassium metal. Elemental analyses were performed at the Elemental Analysis Center of Kyoto University.

2.3. X-ray structure determination

Crystals of **1**, **2** and **3** were grown by slow evaporation of CH_2Cl_2/*n*-hexane (1/2 v/v) solutions. Rigaku AFC7R (for **1** and **2**) and AFC5R (for **3**) diffractometers were used for measurement of diffraction data with graphite monochromated Mo Kα radiation ($\lambda = 0.71069$ Å). A Rigaku XR-TCS-2-050 temperature controller was used for low temperature measurements. All structures were solved and refined using the TEXSAN® crystallographic software package [26]. Scattering factors for neutral atoms were from Cromer and Waber [27] and anomalous

Table 1
Crystal data and refinement description

	1	**2**	**3**
Chemical formula	$C_{29}H_{25}Rh_3$	$C_{29}H_{25}CoRh_2$	$C_{29}H_{25}Co_2Rh$
Molecular weight	682.23	638.26	594.29
Crystal size (mm)	$0.50 \times 0.44 \times 0.23$	$0.47 \times 0.33 \times 0.03$	$0.56 \times 0.46 \times 0.05$
Crystal system	monoclinic	monoclinic	monoclinic
Space group	$P2_1/a$ (no. 14)	$P2_1/a$ (no. 14)	$P2_1/a$ (no. 14)
a (Å)	17.959((6)	17.692(2)	17.710(2)
b (Å)	14.938(7)	14.991(2)	14.958(1)
c (Å)	18.424(5)	18.691(2)	18.471(3)
β (°)	107.79(2)	108.751(7)	108.51(1)
V (Å^3)	4706(2)	4693.9(8)	4639.9(10)
Z	8	8	8
d (calcd) (g cm^{-3})	1.926	1.806	1.701
μ (cm^{-1})	20.90	21.00	21.30
T (°C)	-125 ± 2	23 ± 1	23 ± 1
2θ limit (°)	55	55	60
Reflection measured	11588	11559	14868
Unique reflections	10816	10788	13924
Reflections with $I > 2\sigma(I)$	9099	7019	9495
R_1, R_w[a]	0.029, 0.068	0.043, 0.081	0.034, 0.069
GOF	1.63	1.20	1.23
Residual (min, max)	−1.21, 0.55	−0.73, 0.76	−0.49, 0.65

[a] $R_1 = \sum ||F_o| - |F_c|| / \sum |F_o|$ for reflections with $I > 2\sigma(I)$, $R_w = [(\sum w(F_o^2 - F_c^2)^2 / \sum w(F_o^2)^2)]^{1/2}$ for all data.

dispersion [28] was used. Positions of the metal atoms were determined by direct methods (SHELXS-86 [29]). An analytical absorption correction [30] was applied for **2** and **3**, and a psi-scan correction [31] for **1**. Rhodium and one of two cobalt atoms were disordered in both of the two independent molecules in **3**. Sites $M(11)$ and $M(12)$ were refined as nCo + $(1-n)$Rh and $(1-n)$Co + nRh, respectively ($M(11)$ 66% Rh, 34% Co; $M(12)$ 34% Rh, 66% Co). Sites $M(21)$ and $M(22)$ were treated similarly ($M(21)$ 71% Rh, 29% Co; $M(22)$ 29% Rh, 71% Co). Cyclopentadienyl ligands on Co(23) in **2** and Co(23) in **3** were disordered and refined by using rigid groups. The final least-square cycle included non-hydrogen atoms with anisotropic thermal parameters and hydrogen atoms at fixed positions with isotropic thermal parameters, which were 1.2 times greater than those of the connected atoms. The crystal data and description of the structure refinement are summarized in Table 1.

2.4. DFT calculation

Geometry optimization was performed on the restricted DFT with the B3LYP formulation [32–34] by using the GAUSSIAN 98 program [35]. The effective core potentials (ECPs) and the basis functions for the Co and Rh atoms were those of LANL2DZ (split-valence type) [36]. The 6-31G split-valence set was used for the C and H atoms [37]. The d functions were of the mutually orthogonal five-function type. The geometries of model complex **1′**, **2′** and **3′** were optimized in C_s symmetries of which the mirror plane includes one metal atom (rhodium for **1′** and **3′** and cobalt for **2′**) and capping CH groups and is perpendicular to the M_3 plane. To calculate the absorption spectra of **1′**, TDDFT [38,39] was used with ECP and basis functions of LANL2DZ for the metal atoms and those of 6-31G* for C and H atoms at the geometries optimized by the above-mentioned method. The absorption spectrum of **4′** was also calculated with a similar method to that for **1** at the optimized geometries in [40].

3. Results and discussion

3.1. Synthesis and structure

The trirhodium cluster **1** was synthesized by a similar method to that of **4** by using $[CpRh(CO)_2]$ instead of $[CpCo(CO)_2]$. The reaction of the mixture of $[CpRh(CO)_2]$ and $[CpCo(CO)_2]$ with diphenylacetylene gave a mixture of homo- and mixed-metal trinuclear clusters $[Co_{3-n}Rh_nCp_3(\mu_3\text{-}CPh)_2]$ (**1**, **2**, **3** and **4**). A 1:2.4 mole ratio of the mononuclear starting Rh- and Co-complexes gave every trinuclear cluster of which the mole ratios were close to the statistical ones. Careful chromatographic separation on a silica-gel column was needed to isolate each of the trinuclear clusters. The product collected as **2** by the silica-gel chromatographic separation was inevitably contaminated with some colorless crystals of hexaphenylbenzene derived from diphenylacetylene. The pure sample of **2** was separated from the contaminant by gel-permeation chromatography.

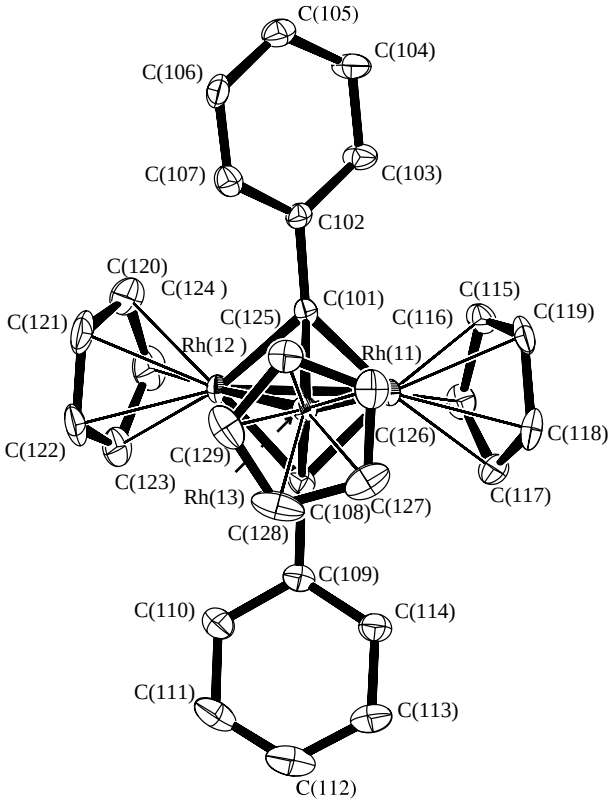

Fig. 1. ORTEP drawing of $[Rh_3Cp_3(\mu_3\text{-}CPh)_2]$ (**1**) with 50% probability. Hydrogen atoms are omitted for clarity.

The trirhodium complex **1** and the mixed-metal complexes **2** and **3** crystallized in isostructural monoclinic unit cells. These crystals have two independent molecules in a unit cell. The structure of one of the two independent molecules in the crystal of **1** is shown in Fig. 1 with an atom numbering scheme. A similar atom-numbering scheme is adopted for each independent molecule in all structures. [1] In the crystal of **2**, the cobalt atoms occupy the $M(13)$ and $M(23)$ positions in each independent molecule and the rhodium atoms occupy the other metal-atom sites. In that of **3**, one of the two cobalt atoms in each independent molecule also occupies sites $M(13)$ and $M(23)$, respectively. The other cobalt and the rhodium atoms are disordered at the other metal atom sites, $M(11)$ and $M(12)$, and $M(21)$ and $M(22)$.

Important distances of all complexes are listed in Table 2. Average bond distances are summarized in Table 3. The average Rh—Rh distance in trirhodium

[1] The first digits in the parentheses are used to distinguish the independent molecules for **1**, **2** and **3**.

Table 2
Selected bond distances (Å) in $[M_3Cp_3(\mu_3\text{-}CPh)_2]$ (M_3: Rh_3, **1**; $CoRh_2$, **2**; Co_2Rh, **3**)

	1[a]	**2**[b]	**3**[c]
M(11)—*M*(12)	2.6177(4)	2.6092(7)	2.4899(4)
M(11)—*M*(13)	2.6119(7)	2.4977(8)	2.4561(5)
M(12)—*M*(13)	2.6212(6)	2.507(1)	2.4384(7)
M(21)—*M*(22)	2.6319(4)	2.6247(7)	2.5000(4)
M(21)—*M*(23)	2.6346(5)	2.5231(8)	2.4957(4)
M(22)—*M*(23)	2.6004(6)	2.4859(9)	2.4044(5)
M(11)—C(101)	1.995(4)	1.982(6)	1.950(3)
M(11)—C(108)	1.987(4)	1.985(5)	1.960(3)
M(12)—C(101)	1.997(4)	1.990(6)	1.916(3)
M(12)—C(108)	1.980(4)	1.957(7)	1.901(4)
M(13)—C(101)	1.976(4)	1.873(6)	1.862(3)
M(13)—C(108)	1.987(4)	1.873(7)	1.873(3)
M(21)—C(201)	2.003(4)	1.996(7)	1.952(3)
M(21)—C(208)	1.992(4)	1.992(6)	1.952(3)
M(22)—C(201)	1.997(4)	1.987(6)	1.912(3)
M(22)—C(208)	1.989(4)	1.983(7)	1.910(4)
M(23)—C(201)	1.990(4)	1.882(6)	1.873(3)
M(23)—C(208)	1.988(4)	1.886(6)	1.870(3)
C(101)—C(102)	1.477(5)	1.481(9)	1.475(4)
C(108)—C(109)	1.471(5)	1.476(9)	1.469(4)
C(201)—C(202)	1.464(5)	1.479(9)	1.475(5)
C(208)—C(209)	1.472(5)	1.466(9)	1.472(5)

[a] All *M* atoms are rhodium.
[b] *M*(11), *M*(12), *M*(13) and *M*(23) are rhodium. *M*(13) and *M*(23) are cobalt.
[c] Disorders: *M*(11) = 34% Co + 66% Rh; *M*(12) = 66% Co + 34% Rh; *M*(21) = 29% Co + 71% Rh; *M*(22) = 71% Co + 29% Rh. *M*(13) and *M*(23) are cobalt.

Table 3
Selected average bond distances (Å) in $[M_3Cp_3(\mu_3\text{-}CPh)_2]$ (M_3: Rh_3, **1**; $CoRh_2$, **2**; Co_2Rh, **3**; Co_3, **4**) and in DFT-optimized geometries of $[M_3Cp_3(\mu_3\text{-}CH)_2]$ (M_3: Rh_3, **1′**; $CoRh_2$, **2′**; Co_2Rh, **3′**; Co_3, **4′**)

	Rh_3	$CoRh_2$	Co_2Rh	Co_3
X-ray	**1**	**2**	**3**	**4**[b,c]
Rh—Rh	2.620(13)	2.617(8)		
Co—Rh		2.503(16)	[a]	
Co—Co			[a]	2.382(8)
Rh—C(cap)	1.990(7)	1.984(12)	[a]	
Co—C(cap)		1.878(7)	1.870(5)	1.871(5)
Rh—C(Cp)	2.233(19)	2.233(18)	[a]	
Co—C(Cp)		2.073(18)	2.078(12)	2.081(8)
DFT	**1′**	**2′**	**3′**	**4′**[b]
Rh—Rh	2.677	2.680		
Co—Rh		2.548	2.548	
Co—Co			2.430	2.429
Rh—C(cap)	2.004	1.994	1.986	
Co—C(cap)		1.879	1.868	1.861
Rh—C(Cp)	2.347	2.349	2.352	
Co—C(Cp)		2.151	2.151	2.150

[a] Not determined because of disordering cobalt and rhodium atoms.
[b] Ref. [40].
[c] Averaged values over two types of crystals, triclinic and orthorhombic form; for details see [40].

complex **1** is 2.620(13) Å, which is similar to that in $[Rh_3Cp^*_3(\mu_3\text{-}CH)_2]$ (2.6363(5) Å) [23].

The Rh—Rh distance in **2** (2.617(8) Å) is quite similar to those in **1**. The Co—Rh distance in **2** (2.503(16) Å) is close to the average of the Co—Co distance in **4** [40] and the Rh—Rh distance in **1**, 2.501 Å. The Co—C(cap) distance of **2** and **3** and the Rh—C(cap) distance of **2** are also similar to those in **4** and **1**, respectively. These data indicate that the metal–metal bond distances in these trinuclear clusters are rather insensitive to any special effect for making a bond between heterometal atoms. The C(cap)—Ph distances for all of the current complexes are identical to each other within experimental errors.

3.2. Properties

The ^{1}H NMR chemical shifts of the Cp ligand for homometal clusters **1** and **4** were 5.06 and 4.43 ppm, respectively. Cluster **2** absorbed two peaks in this region at 5.15 and 4.28 ppm in an intensity ratio of 2:1. This intensity ratio shows the more intense 5.15 ppm peak is due to the Cp moieties connected to the rhodium atoms and the 4.28 ppm peak arises from the Cp ligand on the cobalt atom. The peaks of a 1:2 intensity ratio for **3** lead to the assignment of a 5.16 ppm peak to the Cp group bound to the rhodium atom and a 4.39 ppm peak to those bound to the cobalt atoms. The ^{13}C NMR peaks for the Cp connected to the rhodium atoms shifted slightly toward the lower field with the decrease of the number of rhodium atoms (86.9, 87.1 and 87.4 ppm for **1**, **2** and **3**, respectively). The peaks for those connected to the cobalt atoms shifted to the lower field also by decreasing the number of rhodium atoms (84.9, 84.9 and 85.5 ppm for **2**, **3** and **4**, respectively). Proton peaks of the phenyl group are shifted to the higher field by increasing the number of rhodium atoms (e.g., chemical shifts of *o*-Ph for **1**, **2**, **3** and **4** were 7.71, 7.87, 8.06 and 8.30 ppm, respectively).

Fig. 2 shows the cyclic voltammograms of the current trinuclear clusters in MeCN. Complexes **2**, **3** and **4** showed a chemically reversible oxidation and a chemically reversible reduction process. Complex **1** also showed a chemically reversible reduction wave, but its oxidation response was irreversible. In the CH_2Cl_2 solution of **1**, two successive chemically reversible oxidation waves were observed. For **4**, both of the oxidation and reduction responses are one-electron processes [21]. For **2** and **3**, coulometry experiments showed that their oxidation waves are one-electron processes. Because the peak current value of the reduction is similar to that for the oxidation response, the reduction for **2** and **3** should be also a one-electron process. The reduction of **1** is concluded as a one-electron process by comparison of the peak current value with that of **4** as an internal standard. The oxidation responses of **1** in CH_2Cl_2 were also assigned as two one-electron processes. Redox potentials of all four complexes are summarized in Table 4. The one-electron oxidation and reduction responses are shifted to more negative and more positive potentials, respectively, with the decrease of the number of the rhodium atom. These data indicate that the energy of HOMO becomes higher and that of LUMO lower with the decrease of the number of rhodium atoms.

The anionic radical of **3** was generated by contact of its MTHF solution with potassium metal under a vacuum at room temperature, similarly to the generation of anionic radical of **4** [21]. The room-temperature fluid-solution ESR spectra of $\mathbf{3}^{-\cdot}$ is shown in Fig. 3. A reliable ESR spectra of $\mathbf{1}^{-\cdot}$ and $\mathbf{2}^{-\cdot}$ could not be obtained by this method probably due to their insufficient lifetimes for

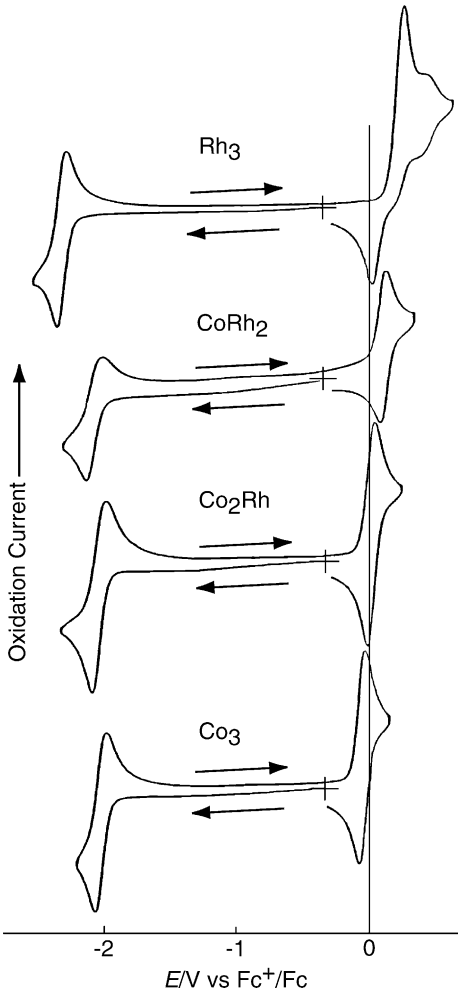

Fig. 2. Cyclic voltammogram of $[M_3Cp_3(\mu_3\text{-}CPh)_2]$ in MeCN.

Table 4
Electrochemical data of $[M_3Cp_3(\mu_3\text{-}CPh)_2]$ in MeCN

	$E_{1/2}$ (V) vs. Fc^+/Fc		
	0/−1	+1/0	+2/+1
1	−2.34[a]	+0.24[a,b]	+0.51[b,c]
2	−2.10[a]	+0.10[a]	
3	−2.05[a]	+0.03[a]	
4	−2.05[a]	−0.06[a]	

[a] Chemically reversible one-electron process.
[b] In CH_2Cl_2.
[c] Irreversible process; anodic peak potential.

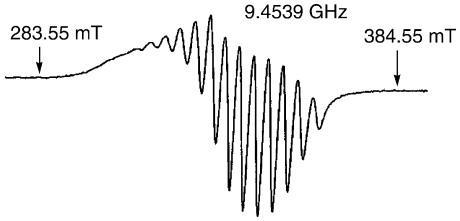

Fig. 3. ESR spectrum of $\mathbf{3}^-$ in MTHF solution at room temperature.

sample transfer for ESR measurements. The spectrum of $\mathbf{3}^{-\cdot}$ is a 15-fold multiplet of 39.6×10^{-4} cm^{-1} due to two equivalent ^{59}Co nuclei (100% natural abundance, $I = 7/2$) centered at $g = 2.031$. Hyperfine splittings due to ^{103}Rh (100% natural abundance, $I = 1/2$) were not resolved because of its very small nuclear magnetic moment [41]. The hyperfine coupling constant of ^{59}Co nuclei of $\mathbf{3}^{-\cdot}$ is slightly smaller than that of $\mathbf{4}^{-\cdot}$. The g values and hyperfine constants are summarized in Table 5.

Fig. 4 shows the electronic absorption spectra of the current four complexes in CH_2Cl_2. Complex **4** has a weak shoulder band at 740 nm with $\varepsilon = 332$ mol^{-1} L cm^{-1}. Complexes **3** and **2** also have a weak absorption band (shoulder) at 665 and 565 nm, respectively. No corresponding peak or shoulder was observed for **1** in the long wavelength region. Four or five bands were observed in the shorter wavelength region than 550 nm for the current complexes. The assignment of the visible-region bands for the homometal clusters will be discussed later.

3.3. Electronic structure

Geometry optimization was made for the model complexes of **1′**, **2′** and **3′** in C_s symmetry by using the B3LYP DFT method. Optimized geometries of them and **4′** [40] are summarized in Table 3 with the average bond distances of molecular structures of $[M_3Cp_3(\mu_3\text{-}CPh)_2]$. The Rh_3C_2 skeleton for optimized **1′** had a pseudo-D_{3h} symmetry. The corresponding ones for **2′** and **3′** had a pseudo-C_{2v} symmetry. We use the symmetry label of these highly symmetric point groups in the discussion below. The optimized Rh—Rh distance in **2′** and the Co—Co distance in **3′** are very similar to those calculated for each homometal model complex. The Rh—Co distance in **2′** and **3′** is nearly equal to the sum of the halves of the calculated homometal M—M distances. The optimized metal–metal lengths for **1′**–**3′** have reproduced those observed for **1**–**3**, but the bonds optimized with the present method are 0.045–0.063 Å longer than the observed ones. The optimized Co—Co bond length was also 0.047 Å longer than that in **4** [40]. The Rh—C(cap) and Co—C(cap) distances are constant throughout the calculated model complexes. These results are consistent with the experimental observations.

Table 5
Isotropic ESR data of $[M_3Cp_3(\mu_3\text{-}CPh)_2]^-$ in fluid MTHF

Radical	$\langle g \rangle$	$\langle a(\mathrm{Co}) \rangle / 10^{-4}$ cm^{-1}
$\mathbf{3}^{-\cdot}$	2.031	−39.6
$\mathbf{4}^{-\cdot}$[a]	2.035	−40.9

[a] Ref. [21].

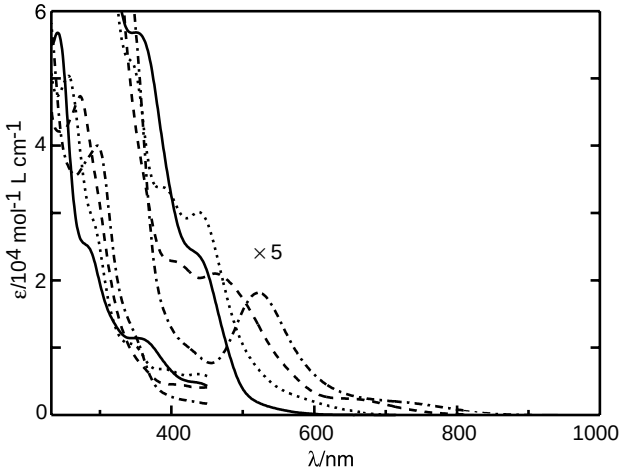

Fig. 4. Electronic absorption spectra of **1** (solid line), **2** (dotted line), **3** (broken line) and **4** (broken line with dots) in CH_2Cl_2.

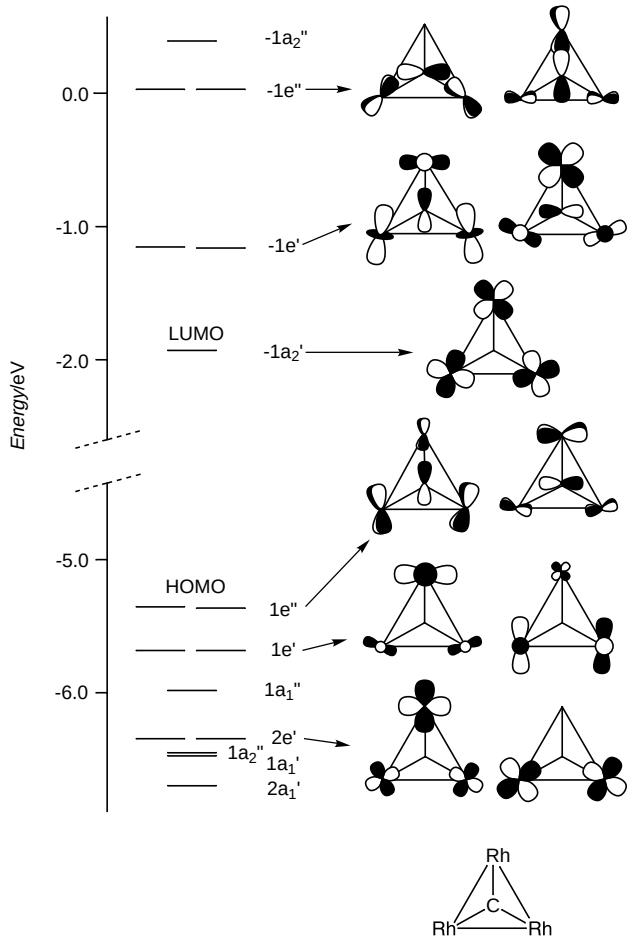

Fig. 5. Orbital energy diagram and schematic representation of orbitals around the HOMO–LUMO levels of **1′**. The orbital symmetry notations are based on an idealized D_{3h} point group.

An energy level diagram near the HOMO–LUMO levels of **1′** is shown in Fig. 5. [2] For all four complexes, **1′**–**4′**, the LUMO is an in-plane M–M antibonding a_2' in

[2] The occupied orbitals are numbered downward from the HOMO for each symmetry label with a positive number. The virtual orbitals are numbered upward from the LUMO with a negative number.

Table 6
Electronic absorption spectral data for **1** and **4** and transition energies calculated by TDDFT for **1′** and **4′**

Observed			Calculated				
ΔE (eV)	λ (nm)[a]	ϵ (mol^{-1} L cm^{-1})	ΔE (eV)	λ (nm)	o.s.[b]	Transition[c]	w.t.[d]
1			**1′**				
2.76	450sh	4380	2.958	419	0.1134	$1e' \rightarrow -1a_2'$	0.65
3.40	365sh	10,900	3.723	333	0.2258	$1e' \rightarrow -1e'$	0.58
4			**4′**				
1.68	740sh	332	2.020	614	0.0033	$2e' \rightarrow -1a_2'$	0.38
						$1e' \rightarrow -1a_2'$	0.26
2.38	522	3650	2.419	513	0.0130	$1e' \rightarrow -1a_2'$	0.25
						$2e' \rightarrow -1a_2'$	0.21
2.88	430sh	1970	3.398	365	0.0639	$1e'' \rightarrow -1e''$	0.29
						$1e' \rightarrow -1a_2'$	0.27
						$1e' \rightarrow -1e'$	0.16
3.59	345sh	12,000	3.516	353	0.0216	$1e' \rightarrow -1e'$	0.36
						$1e'' \rightarrow -1a_2''$	0.27

[a] sh: Shoulder.
[b] Oscillator strength.
[c] Major transition character, based on D_{3h} point group.
[d] Weight of transition.

D_{3h} or b_1 in C_{2v} (a″ orbital in C_s). The a_2' orbital is also LUMO for **4′** [40] and is consistent with the experimentally determined one for **4** from the analysis of the ESR spectra of its anionic radical [21]. The HOMOs are degenerate and out-of-plane metal–metal bonding (π_{MM} and δ_{MM}) and metal–C(cap) anti-bonding orbitals, which are e″ (in D_{3h}, see Fig. 5) or the corresponding nearly degenerate a_2 and b_2 (in C_{2v}) orbitals. The CV data suggests that the energy of the HOMO is higher and that of the LUMO is lower for the cobalt-richer complexes in **1**–**4**. These orbital energy changes were not reproduced in our DFT calculations for **1′**–**4′**.

The electronic absorption spectra of the model complexes of homometal **1′** and **4′** clusters were calculated by using the TDDFT method and compared with those of **1** and **4** (Table 6). Because the observed absorption bands in the higher energy region may include those of the benzylidyne origin, we discuss here the bands lower than 4 eV ($\lambda > 310$ nm). The calculated excitation energies and oscillator strengths are shown in Fig. 6 together with the observed spectra of **1** and **4**. As summarized in Table 6 each of the low-energy excitations of **1′** was expressed by a predominant single transition, whereas those for **4′** were obtained as a combination of two or three transitions mixed with similar weights. The HOMO (1e″) to LUMO ($-1a_2'$) transition for **1′** is forbidden under the D_{3h} symmetry. The two lowest-energy intense excitations were calculated as 2.96 eV (419 nm) and 3.72 eV (333 nm), which agree well with the observed shoulder, bands at 2.76 eV (450 nm) and 3.40 eV (365 nm) of **1**, respectively. Both are symmetry-allowed transitions. The former is mainly the 1e′ to LUMO, and the latter is the 1e′ to $-1e'$ transition. These are transitions predominantly within the RhRh bond system.

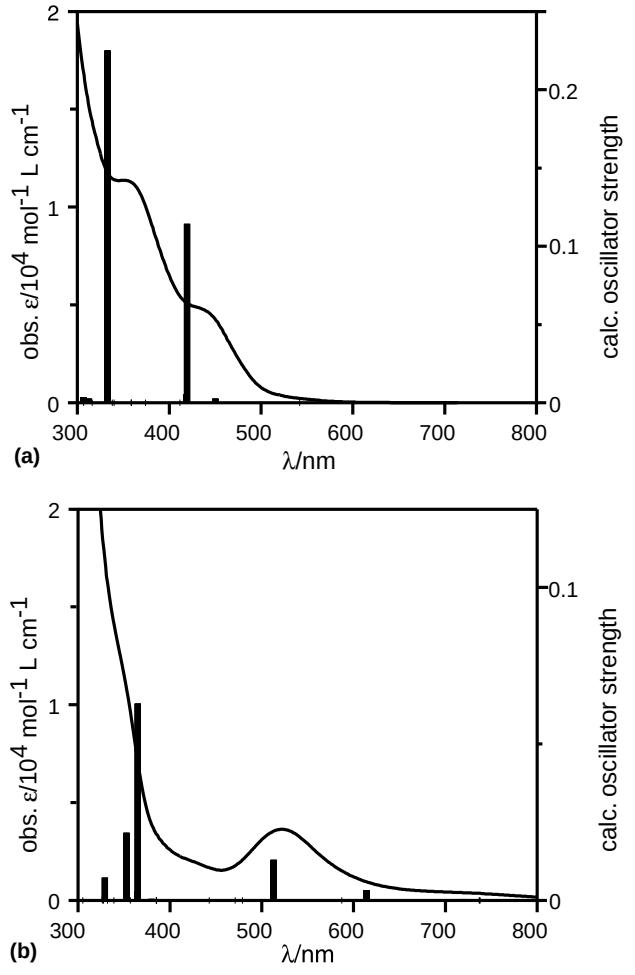

Fig. 6. UV–Vis absorption spectra of (a) **1** and (b) **4** and calculated absorption bands (sticks) of (a) **1′** and (b) **4′**.

In the calculated spectrum of the tricobalt cluster, **4′**, there are four bands in this region. The lowest energy excitation was calculated at 2.02 eV (614 nm) with a small oscillator strength. The main contribution to this band was the 2e′ orbitals to LUMO ($-1a_2'$) transition. The shoulder band at 1.68 eV (740 nm) in the observed spectrum of **4** may be assigned to this excitation. The corresponding excitation of **1′** was calculated at 2.76 eV (450 nm) with a small oscillator strength of 0.003, that is close to the calculated intense excitation at 2.96 eV (419 nm). Thus, we suppose this band was not resolved in the spectrum of **1**. The calculated absorption band at 2.42 eV (513 nm) for **4′** includes the 1e′ to LUMO ($-1a_2'$) transition that is similar to the lowest-energy intense band in **1′**, but the band for **4′** also includes a transition character from the lower 2e′ orbitals to the LUMO ($-1a_2'$).

The energy of this excitation agrees reasonably with the observed band at 2.38 eV (522 nm) of **4**. The band at 3.40 eV (365 nm) of **4′** corresponds to the 3.72 eV (333 nm) band of **1′**. However, in addition to the 1e′ to $-1e'$ transition, the band for **4′** includes the HOMO (1e″) to $-1e''$ and the 1e′ to LUMO ($-1a_2'$) transitions. The band calculated at 3.52 eV (353 nm) includes the 1e′ to $-1e'$ and 1e″ to $-1a_2''$ transitions. The observed band (shoulder) at 2.88 eV (430 nm) and 3.59 eV (345 nm) for **4** may be assigned to these transitions. Simpson and coworkers examined the absorption spectra of the tricobalt complexes with various capping ligands [22]. They reported that the absorption band around 500 nm is not affected by the capping ligands, whereas the band between 360 and 430 nm depends on the capping ligands. These are consistent with our calculations that the former band corresponds to the transition between the orbitals with no or small capping carbon characters and the latter includes the orbitals with appreciable capping carbon character.

4. Concluding remarks

Reduction and oxidation potentials of **1**–**4** shifted to more negative and more positive ones, respectively, with the increase of the number of the rhodium atoms. In the UV–Vis absorption spectra the lowest-energy intense band blue-shifted also with the increase of the rhodium-atom number. A simplest interpretation for these experimental results is that as a cobalt atom is replaced by a rhodium atom the HOMO and LUMO energies shift upward and downward, respectively. We could not see this simple picture in the energy levels or vertical energy differences accompanying the addition or subtraction of an electron in the DFT calculations with the current parameterization. However, we emphasize that the UV–Vis excitation energy of **1′** and **4′** calculated by the TDDFT method semi-quantitatively reproduced the UV–Vis spectrum of **1** and **4**.

5. Supplementary material

Crystallographic data (excluding structure factors) for the structural analysis have been deposited with the Cambridge Crystallographic Data Centre, CCDC Nos. 201477–201479 for **1**, **2** and **3**, respectively. Copies of this information may be obtained free of charge from The Director, CCDC, 12 Union Road, Cambridge, CB2 1EZ, UK [Fax: +44-1223-336033; e-mail: deposit@ccdc.cam.ac.uk or www: http://www.ccdc.cam.ac.uk]. Tables of Cartesian coordinates of the DFT optimized geometries of **1′**, **2′** and **3′** and ground state TDDFT vertical excitation energies and oscillator strengths of **1′** and **4′** are available on request from the author (T.K.).

Acknowledgements

This work was supported by Grants-in-Aid for Scientific Research from the Ministry of Education, Culture, Sports, Science and Technology of Japan. DFT and TDDFT calculations were performed on an SGI Origin 3400 at the Gifu University Computer Center.

References

[1] H. Wadepohl, S. Gebert, Coord. Chem. Rev. 143 (1995) 535.
[2] V.A. Uchtman, L.F. Dahl, J. Am. Chem. Soc. 91 (1969) 3763.
[3] P.D. Frisch, L.F. Dahl, J. Am. Chem. Soc. 94 (1972) 5082.
[4] R.F. Bedard, L.F. Dahl, J. Am. Chem. Soc. 108 (1986) 5933.
[5] M.S. Ziebarth, L.F. Dahl, J. Am. Chem. Soc. 112 (1990) 2411.
[6] C.R. Pulliam, J.B. Thoden, A.M. Stacy, B. Spencer, M.H. Englert, L.F. Dahl, J. Am. Chem. Soc. 113 (1991) 7398.
[7] K.A. Kubat-Martin, A.D. Rae, L.F. Dahl, Organometallics 4 (1985) 2221.
[8] W.L. Olson, A.M. Stacy, L.F. Dahl, J. Am. Chem. Soc. 108 (1986) 7646.
[9] W.L. Olson, L.F. Dahl, J. Am. Chem. Soc. 108 (1986) 7657.
[10] R.L. Bedard, A.D. Rae, L.F. Dahl, J. Am. Chem. Soc. 108 (1986) 5924.
[11] R.F. Bedard, L.F. Dahl, J. Am. Chem. Soc. 108 (1986) 5942.
[12] N. Kamijo, T. Watanabe, Acta Crystallogr., Sect. B 35 (1979) 2537.
[13] J.R. Fritch, K.P.C. Vollhardt, M.R. Thompson, V.W. Day, J. Am. Chem. Soc. 101 (1979) 2768.
[14] H. Yamazaki, Y. Wakatsuki, K. Aoki, Chem. Lett. (1979) 1041.
[15] S.B. Colbran, L.R. Hanton, B.H. Robinson, W.T. Robinson, J. Simpson, J. Organometal. Chem. 330 (1987) 415.
[16] H. Wadepohl, H. Pritzkow, Polyhedron 8 (1989) 1939.
[17] S.M. Elder, B.H. Robinson, J. Simpson, J. Organometal. Chem. 398 (1990) 165.
[18] J.R. Fritch, K.P.C. Vollhardt, Angew. Chem., Int. Ed. Engl. 19 (1980) 559.
[19] D.E. Van Horn, K.P.C. Vollhardt, J. Chem. Soc., Chem. Commun. (1982) 203.
[20] K.P.C. Vollhardt, E.C. Walborsky, J. Am. Chem. Soc. 105 (1983) 5507.
[21] S. Enoki, T. Kawamura, T. Yonezawa, Inorg. Chem. 22 (1983) 3821.

[22] S.B. Colbran, B.H. Robinson, J. Simpson, Organometallics 3 (1984) 1344.
[23] A.V. DeMiguel, K. Isobe, P.M. Bailey, N.J. Meanwell, P.M. Maitlis, Organometallics 1 (1982) 1604.
[24] M.D. Rausch, R.A. Genetti, J. Org. Chem. 35 (1970) 3888.
[25] B.G. Conway, M.D. Rausch, Organometallics 4 (1985) 688.
[26] teXsan: Crystal Structure Analysis Package 1.11, Molecular Structure Corporation: Woodland, TX, 2000.
[27] D.T. Cromer, J.T. Waber, in: J.A. Ibers, W.C. Hamilton (Eds.), International Tables for X-ray Crystallography, vol. IV, Kynoch Press, Birmingham, 1974.
[28] D.C. Creagh, W.J. McAuley, in: A.J.C. Wilson (Ed.), International Tables for X-ray Crystallography, vol. C, Kluwer Academic Publishers, Boston, MA, 1992, p. 219.
[29] G.M. Sheldrick, in: G.M. Sheldrick, C. Kruger, R. Goddard (Eds.), Crystallographic Computing 3, Oxford University Press, Oxford, 1985, p. 175.
[30] J. De Meulenaer, H. Tompa, Acta Crystallogr. 19 (1965) 1014.
[31] A.C.T. North, D.C. Phillips, F.S. Mathews, Acta Crystallogr., Sect. A 24 (1968) 351.
[32] A.D. Becke, J. Chem. Phys. 98 (1993) 5648.
[33] B. Miehlich, A. Savin, H. Stoll, H. Preuss, Chem. Phys. Lett. 157 (1989) 200.
[34] C. Lee, W. Yang, R.G. Parr, Phys. Rev. B 37 (1988) 785.
[35] M.J. Frisch, G.W. Trucks, H.B. Schlegel, G.E. Scuseria, M.A. Robb, J.R. Cheeseman, V.G. Zakrzewski, J.J.A. Montgomery, R.E. Stratmann, J.C. Burant, S. Dapprich, J.M. Millam, A.D. Daniels, K.N. Kudin, M.C. Strain, O. Farkas, J. Tomasi, V. Barone, M. Cossi, R. Cammi, B. Mennucci, C. Pomelli, C. Adamo, S. Clifford, J. Ochterski, G.A. Petersson, P.Y. Ayala, Q. Cui, K. Morokuma, P. Salvador, J.J. Dannenberg, D.K. Malick, A.D. Rabuck, K. Raghavachari, J.B. Foresman, J. Cioslowski, J.V. Ortiz, A.G. Baboul, B.B. Stefanov, G. Liu, A. Liashenko, P. Piskorz, I. Komaromi, R. Gomperts, R.L. Martin, D.J. Fox, T. Keith, M.A. Al-Laham, C.Y. Peng, A. Nanayakkara, M. Challacombe, P.M.W. Gill, B. Johnson, W. Chen, M.W. Wong, J.L. Andres, C. Gonzalez, M. Head-Gordon, E.S. Replogle, J.A. Pople, Gaussian 98 A.11.1, Gaussian, Inc., Pittsburgh, PA, 2001.
[36] P.J. Hay, W.R. Wadt, J. Chem. Phys. 82 (1985) 299.
[37] R. Ditchfield, W.J. Hehre, J.A. Pople, J. Chem. Phys. 54 (1971) 724.
[38] R. Bauernschmitt, R. Ahlrichs, Chem. Phys. Lett. 256 (1996) 454.
[39] R.E. Stratmann, G.E. Scuseria, M.J. Frisch, J. Chem. Phys. 109 (1998) 8218.
[40] M. Ebihara, M. Iiba, M. Kato, H. Minami, T. Kawamura, Inorg. Chim. Acta (2004), in press.
[41] J.A. Pople, W.G. Scneider, H.J. Bernstein, High-resolution Nuclear Magnetic Resonance, McGraw-Hill, New York, 1959.